Perturbation-Based Spectral Stochastic Meshless Local Petrov-Galerkin Method in Predicting Probabilistic Settlements

Guang Yih Sheu[*,§]

Department of Accounting Information System, Chang-Jung Christian University, Kway-Jen, Tainan 714, Taiwan

Abstract: In an attempt of solving stochastic boundary-value problems sufficiently accurately without creating a finite element discretization, a previous study (Comput. Geotech. 2011, vol. 38, No. 4, pp. 407-415) developed the spectral stochastic meshless local Petrov-Galerkin (SSMLPG) method. Some different approaches of deriving an SSMLPG formulation have been developed using various random field discretization methods. This study presents the SSMLPG formulation composed of perturbation expansions of random fields and a 2D meshfreee weak-strong (MWS) form in elasticity. A performance evaluation of this SSMLPG formulation is implemented through a stochastic elastostatic problem in which probabilistic settlements are predicted with the uncertainty in the spatial variability of Young`s modulus. The evaluation results demonstrate that SSMLPG-based predicted probabilistic settlements approach more close to the Monte Carlo simulation (MCS) results than spectral stochastic finite element-based predicted probabilistic settlements do. In addition, generating the SSMLPG results is time-saving than completing the MCS does. In conclusion, the SSMLPG method can be an efficient alternative tool to solve stochastic boundary-value problems.

Keywords: Spectral stochastic meshless local Petrov-Galerkin method, perturbation expansion, meshfree weak-strong formulation, uncertainty.

1. INTRODUCTION

Solving computational mechanic problems may encounter the uncertainties contributed by such as the spatial variability of material properties and complex scenarios of imposed loadings. Accounting for such uncertainties is necessary, since these uncertainties can cause unreliable numerical results for the design purpose.

One of the approaches for solving computational mechanic problems with accounting for the possible uncertainties is assuming random fields to represent those uncertainties and regarding the corresponding computational mechanic problem as a stochastic boundary-value problem. To solve a stochastic boundary-value problem, we can apply the spectral stochastic finite element (SSFEM) method [1]. Briefly, deriving an SSFEM formulation couples a conventional finite element formulation with the representations of random fields. These representations of random fields can be derived by such as the perturbation and Karhunen-Loève expansions.

A number of SSFEM formulations are available for some branches of engineering. References [2-3] are two recent examples. However, some other studies; for example, Ref. [4], reported deficiencies, such as mesh distortion under large deformations or re-meshing around the crack tip in the crack propagation, in applying the SSFEM method. To eliminate these deficiencies thereby improve the computational efficiency, a previous study [5] extended the meshless local Petrov-Galerkin (MLPG) method [6] to the SSMLPG method. Applying the SSMLPG method does not need a finite element discretization. Therefore, the time spent to create a finite element discretization or background cells for the numerical integration can be saved. Nonetheless, the SSMLPG results of two elastostatic problems approach more satisfactorily to the MCS results than the SSFEM results of the same problems do [5].

Some different approaches of deriving the SSMLPG formulation have been developed using various random field discretization methods. The succeeding study presents the SSMLPG formulation containing perturbation expansions of random fields and the 2D MWS form in elasticity [7]. In addition, the radial basis function (RBF) is used to construct the meshfree shape function. A performance evaluation of this perturbation-based SSMLPG formulation is implemented through a stochastic elastostatic problem in which probabilistic settlements are predicted subjected to the uncertainty in the spatial variability of Young`s modulus.

The remainder of this study is organized into 4 sections. In Sec. 2, deriving a 2D MWS form in elasticity is reviewed. In Sec. 3, equating the perturbation expansion of Young`s modulus and deducing the perturbation-based SSMLPG formulation is presented. In Sec. 4, a performance evaluation of resulting SSMLPG formulation is implemented. Discussing the evaluation results to draw some conclusion is presented in Sec. 5.

*Address correspondence to this author at the Department of Accounting Information System, Chang Jung Christian University, No. 396, Sec. 1, Chang-Jung Rd., Kway Jen, Tainan, Taiwan; Tel: 886-6-2785123-2225; Fax: 886-6-2785683;
E-mails: xsheu@hotmail.com, xsheu@mail.cjcu.edu.tw

[§]Also Adjunct Associate Professor, Department of Civil Engineering, Feng-Chia University, Taichung, Taiwan.

1874-110X/12 2012 Bentham Open

2. TWO-DIMENSIONAL MESHFREE WEAK-STRONG FORMULATION IN ELASTICITY

Assume linearly elastic and isotropic material and the infinitesimal strain assumption holds. Suppose Ω is a problem domain, $\mathbf{x} = (x_1, x_2)$ is a vector of spatial coordinates, and θ is an event in the probability space. Describe each physical parameter within Ω as functions of $\mathbf{x}$ and θ. This study derives the 2D MWS form in elasticity by the following differential equation:

$$\sigma_{ij,j} + b_i = 0 \tag{1}$$

where σ_{ij} are the stress fields corresponding to the displacement fields u_i, b_i are the body forces, and $(\cdot)_{,j} = \frac{\partial(\cdot)}{\partial x_j}$. The boundary conditions are given by

$$t_i = \sigma_{ij} n_j = \bar{t}_i \quad \text{on the natural boundary } \Gamma_T \tag{2a}$$

$$u = \bar{u}_i \quad \text{on the essential boundary } \Gamma_U \tag{2b}$$

where the overbar represents the prescribed data, t_i are the tractions, n_j are the components of a unit vector $\mathbf{n}$ outward normal to Γ, and $\Gamma = \Gamma_U \cup \Gamma_T$.

Meshfree Strong Form

Suppose there are N_T nodes within Ω. In addition, Ω_S is a local quadrature domain for a node $\mathbf{x}_I$ (I = 1 to N_T) and Γ_S is its boundary. If Ω_S for a node $\mathbf{x}_I$ does not interact with Γ_T, a meshfree strong form of Eq. (1) is applied at this node. We can derive this meshfree strong form by first simplifying σ_{ij} by specific stress-strain and strain-displacement relationships. The resulting expressions are next substituted into Eq. (1). For simplicity, the succeeding study focuses on the plain strain condition; therefore, σ_{ij} are simplified by

$$\begin{Bmatrix} \sigma_{11} \\ \sigma_{22} \\ \sigma_{12} \end{Bmatrix} = \frac{E(1-\nu)}{(1+\nu)(1-2\nu)} \begin{bmatrix} 1 & \frac{\nu}{1-\nu} & 0 \\ \frac{\nu}{1-\nu} & 1 & 0 \\ 0 & 0 & \frac{1-2\nu}{2(1-\nu)} \end{bmatrix} \begin{Bmatrix} \varepsilon_{11} \\ \varepsilon_{22} \\ \varepsilon_{12} \end{Bmatrix}$$
$$= \frac{E(1-\nu)}{(1+\nu)(1-2\nu)} \begin{bmatrix} 1 & \frac{\nu}{1-\nu} & 0 \\ \frac{\nu}{1-\nu} & 1 & 0 \\ 0 & 0 & \frac{1-2\nu}{2(1-\nu)} \end{bmatrix} \begin{bmatrix} \frac{\partial}{\partial x_1} & 0 \\ 0 & \frac{\partial}{\partial x_2} \\ \frac{\partial}{\partial x_2} & \frac{\partial}{\partial x_1} \end{bmatrix} \begin{Bmatrix} u_1 \\ u_2 \end{Bmatrix} \tag{3}$$

where ε_{ij} (i, j = 1 to 2) is the strain field. Substituting Eq. (3) into Eq. (1) results in

$$\begin{aligned} &\frac{E(1-\nu)}{(1+\nu)(1-2\nu)} \left[\frac{\partial^2 u_1}{\partial x_1^2} + \frac{1-2\nu}{2(1-\nu)} \frac{\partial^2 u_1}{\partial x_2^2} + \frac{1}{2(1-2\nu)} \frac{\partial^2 u_2}{\partial x_1 \partial x_2} \right] + b_1 = 0 \\ &\frac{E(1-\nu)}{(1+\nu)(1-2\nu)} \left[\frac{\partial^2 u_2}{\partial x_2^2} + \frac{1-2\nu}{2(1-\nu)} \frac{\partial^2 u_2}{\partial x_1^2} + \frac{1}{2(1-2\nu)} \frac{\partial^2 u_1}{\partial x_1 \partial x_2} \right] + b_2 = 0 \end{aligned} \tag{4}$$

Local Weak Form

If Ω_S for a node $\mathbf{x}_I$ (I = 1 to N_T) interacts with Γ_T, a local weak form of Eq. (1) is applied at this node. Deducing this local weak form initiates from the following equation:

$$\int_{\Omega_S} \left(\sigma_{ij,j} + b_i \right) \beta_I \, d\Omega = 0 \tag{5}$$

where β_I (I = 1 to N_T) is the test function associated with $\mathbf{x}_I$. The succeeding study intends to construct the meshfree shape function ϕ by the RBF; therefore, the resulting ϕ satisfies the Kronecker delta function property ($\phi_{IJ} = 0$ for $I \neq J$, $\phi_{IJ} = 0$ for I = J, and I, J denote two nodes). Consequently, neither Lagrangian multipliers nor penalty parameters are required in Eq. (5) for imposing the essential boundary condition. Meanwhile, simplifying Eq. (5) by the divergence theorem yields

$$\begin{aligned} &\int_{\Omega_S} \sigma_{ij} \beta_{I,j} \, d\Omega - \oint_{L_S} \beta_I t_i \, d\Gamma - \oint_{\Gamma_{SU}} \beta_I t_i \, d\Gamma \\ &= \oint_{\Gamma_{ST}} \beta_I \bar{t}_i \, d\Gamma + \int_{\Omega_S} b_i \beta_I \, d\Omega \end{aligned} \tag{6}$$

where $\Gamma_{ST} = \Omega_S \cap \Gamma_T$, $\Gamma_{SU} = \Omega_S \cap \Gamma_U$, and $L_S = \Gamma_S - \Gamma_{ST} - \Gamma_{SU}$. Theoretically speaking, the shape of Ω_S can be arbitrary in integrating Eq. (6). However, Ω_S can be a rectangle centered at $\mathbf{x}_I$ (I = 1 to N_T) for integrating Eq. (6) more easily. In addition, Ω_s for $\mathbf{x}_I$ may be different from Ω_Q for the same node. Fig. (**1**) outlines the difference between Ω_S and Ω_Q. Moreover, interpolating the distribution of an unknown or a random field can be based on different interpolation domains or points.

Next, β_I (I = 1 to N_T) is set by

$$\beta_I(\mathbf{x}) = \begin{cases} R_I(r_I) & \mathbf{x} \in \Omega_s \\ 0 & otherwise \end{cases} \tag{7}$$

Substituting Eq. (7) into Eq. (6) leads to

$$\begin{aligned} &\int_{\Omega_S} \sigma_{ij} [R_I(\mathrm{r_I})]_{,j} \, d\Omega - \oint_{L_S} [R_I(\mathrm{r_I})] \, t_i \, d\Gamma - \oint_{\Gamma_{SU}} [R_I(\mathrm{r_I})] \, t_i \, d\Gamma \\ &= \oint_{\Gamma_{ST}} [R_I(\mathrm{r_I})] \, \bar{t}_i \, d\Gamma + \int_{\Omega_S} b_i [R_I(\mathrm{r_I})] \, d\Omega \end{aligned} \tag{8}$$

Furthermore, t_i (i = 1, 2) are simplified by Eqs. (2a) and (3). Thus

$$\begin{Bmatrix} t_1 \\ t_2 \end{Bmatrix} = \begin{bmatrix} n_1 & 0 & n_2 \\ 0 & n_2 & n_1 \end{bmatrix} \begin{Bmatrix} \sigma_{11} \\ \sigma_{22} \\ \sigma_{12} \end{Bmatrix}$$
$$= \begin{bmatrix} n_1 & 0 & n_2 \\ 0 & n_2 & n_1 \end{bmatrix} \frac{E(1-\nu)}{(1+\nu)(1-2\nu)} \begin{bmatrix} 1 & \frac{\nu}{1-\nu} & 0 \\ \frac{\nu}{1-\nu} & 1 & 0 \\ 0 & 0 & \frac{1-2\nu}{2(1-\nu)} \end{bmatrix} \begin{bmatrix} \frac{\partial}{\partial x_1} & 0 \\ 0 & \frac{\partial}{\partial x_2} \\ \frac{\partial}{\partial x_2} & \frac{\partial}{\partial x_1} \end{bmatrix} \begin{Bmatrix} u_1 \\ u_2 \end{Bmatrix} \tag{9}$$

Substituting Eq. (9) into Eq. (8) yields

$$\begin{aligned} &\int_{\Omega_S} \mathbf{V}_I^T \mathbf{DBu} \, d\Omega - \oint_{L_S} \mathbf{W}_I \mathbf{nDBu} \, d\Gamma - \oint_{\Gamma_{SU}} \mathbf{W}_I \mathbf{nDBu} \, d\Gamma \\ &= \oint_{\Gamma_{ST}} \mathbf{W}_I \bar{\mathbf{t}} \, d\Gamma + \int_{\Omega_S} \mathbf{W}_I \mathbf{b} \, d\Omega \end{aligned} \tag{10}$$

where $\mathbf{u} = [u_1, u_2]^T$, $\bar{\mathbf{t}} = [\bar{t}_1, \bar{t}_2]^T$, $\mathbf{b} = [b_1, b_2]^T$, and

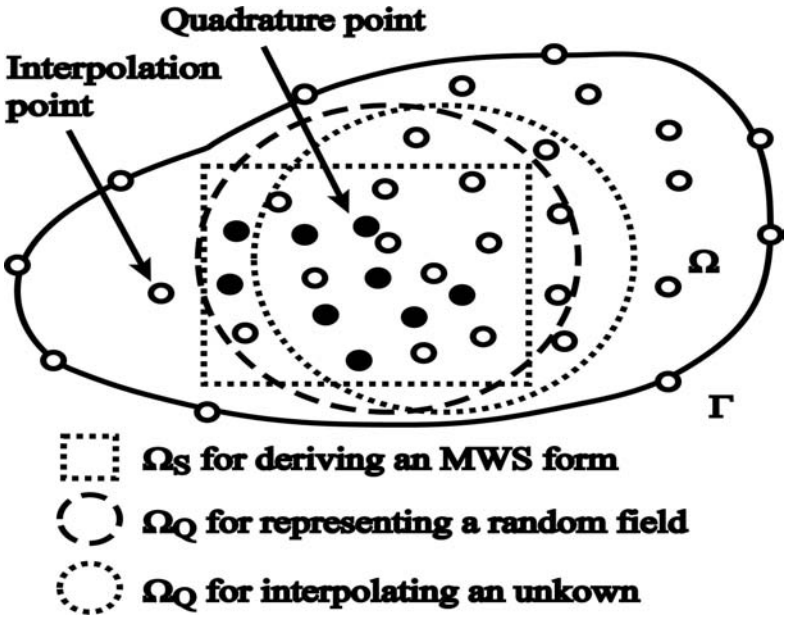

Fig. (1). Difference between Ω_S and Ω_Q.

$$\mathbf{n}=\begin{bmatrix} n_1 & 0 & n_2 \\ 0 & n_2 & n_1 \end{bmatrix},\quad \mathbf{D}=\frac{E(1-\nu)}{(1+\nu)(1-2\nu)}\begin{bmatrix} 1 & \frac{\nu}{1-\nu} & 0 \\ \frac{\nu}{1-\nu} & 1 & 0 \\ 0 & 0 & \frac{1-2\nu}{2(1-\nu)} \end{bmatrix},$$

$$\mathbf{B}=\begin{bmatrix} \frac{\partial}{\partial x_1} & 0 \\ 0 & \frac{\partial}{\partial x_2} \\ \frac{\partial}{\partial x_2} & \frac{\partial}{\partial x_1} \end{bmatrix},\mathbf{V}_I=\begin{Bmatrix} [R_I(r_I)]_{,1} & 0 \\ 0 & [R_I(r_I)]_{,2} \\ [R_I(r_I)]_{,2} & [R_I(r_I)]_{,1} \end{Bmatrix}, \tag{11}$$

$$\mathbf{W}_I=\begin{bmatrix} R_I(r_I) & 0 \\ 0 & R_I(r_I) \end{bmatrix}$$

Discrete Equations

Similarly manipulating the published RBF interpolation formula [5], we can approximate u_i (i = 1, 2) over Ω_Q for $\mathbf{x}_I$ (I = 1 to N_T) by

$$u_i(\mathbf{x},\theta)=\mathbf{\Phi}(\mathbf{x})\mathbf{U}=\sum_{j=1}^{N}\phi_j(\mathbf{x})u_{i,j}(\mathbf{x},\theta) \tag{12}$$

where N is the total number of nodes within Ω_Q, $\mathbf{\Phi}(\mathbf{x})$ = $[\phi_1(\mathbf{x}), \phi_2(\mathbf{x})\ldots\phi_N(\mathbf{x})]$, $\mathbf{U}$ = $[u_{i,1}(\mathbf{x}_1,\theta), u_{i,2}(\mathbf{x}_2,\theta)\ldots u_{i,N}(\mathbf{x}_N,\theta)]^T$. Construction of ϕ for further details can be seen in Ref. [5]. Based on Eq. (12), Eqs. (4) and (10) can be re-written more succinctly in matrix algebra as

$$\mathbf{K}_I\mathbf{u}_I=\mathbf{F}_I \tag{13}$$

where $\mathbf{u}_I=[\mathbf{u}_1,\mathbf{u}_2....\mathbf{u}_N]_I^T$ and $\mathbf{K}_I$ and $\mathbf{F}_I$ are the stiffness and force matrices for $\mathbf{x}_I$ (I = 1 to N_T). $\mathbf{K}_I$ and $\mathbf{F}_I$ are derived by

$$\begin{cases}\mathbf{K}_I=\mathbf{B}^T(\Phi)\mathbf{D}(\mathbf{x})\mathbf{B}(\Phi)\\ \mathbf{F}_I=-\mathbf{b}(\mathbf{x})\end{cases}\qquad(\Omega_Q\cap\Gamma_T=\varnothing) \tag{14a}$$

$$\begin{cases}\mathbf{K}_I=\int_{\Omega_S}\mathbf{V}_I^T\mathbf{DB}(\Phi)\,d\Omega-\oint_{L_S}\mathbf{W}_I\mathbf{nDB}(\Phi)\,d\Gamma\\ \quad\quad-\oint_{\Gamma_{SU}}\mathbf{W}_I\mathbf{nDB}(\Phi)\,d\Gamma\\ \mathbf{F}_I=\oint_{\Gamma_{ST}}\mathbf{W}_I\bar{\mathbf{t}}\,d\Gamma+\int_{\Omega_S}\mathbf{W}_I\mathbf{b}\,d\Omega\end{cases}\qquad(\Omega_Q\cap\Gamma_T\neq\varnothing) \tag{14b}$$

$$\text{in which } \mathbf{B}(\Phi)=\begin{bmatrix} \frac{\partial(\Phi)}{\partial x_1} & 0 \\ 0 & \frac{\partial(\Phi)}{\partial x_2} \\ \frac{\partial(\Phi)}{\partial x_2} & \frac{\partial(\Phi)}{\partial x_1} \end{bmatrix} \tag{14c}$$

Repeat the derivation of Eq. (13) for all N_T nodes and assemble all the resulting equations according to the global numbering system result in

$$\mathbf{K}_{(2N_T\times 2N_T)}\mathbf{u}_{(2N_T\times 1)}=\mathbf{F}_{(2N_T\times 1)} \tag{15}$$

Eq. (15) is not ready for use, since the uncertainty in the spatial variability of E has not been treated. In the next section, representing the spatial variability of E by the perturbation method is presented.

3. THE PERTURBATION METHOD

Theoretical backgrounds of the perturbation method can be consulted with Ref. [8]. Interested readers may refer to this reference.

The first step of deriving the perturbation expansion of E is simulating E as a random field and equating Taylor expansions of $\mathbf{K}$ and $\mathbf{u}$ in terms of fluctuations of E.

Suppose $E_1, E_2 ... E_{N_T}$ are the nodal values of E and small fluctuations $\Delta E_j = E_j - \mu_E$ (j = 1 to N_T) in which μ_E is the mean value of E. The Taylor expansions of $\mathbf{K}$ and $\mathbf{u}$ at ΔE_j = 0 (j = 1 to N_T) are given by

$$\mathbf{K} = \mathbf{K}_0 + \sum_{i=1}^{N_T} \mathbf{K}_{,i}\Delta E_i + \tfrac{1}{2}\sum_{i=1}^{N_T}\sum_{j=1}^{N_T} \mathbf{K}_{,ij}\Delta E_i \Delta E_j + \cdots \tag{16a}$$

$$\mathbf{u} = \mathbf{u}_0 + \sum_{i=1}^{N_T} \mathbf{u}_{,i}\Delta E_i + \tfrac{1}{2}\sum_{i=1}^{N_T}\sum_{j=1}^{N_T} \mathbf{u}_{,ij}\Delta E_i \Delta E_j + \cdots \tag{16b}$$

where

$$\begin{aligned} &\mathbf{K}_0 = \mathbf{K}(E=\mu_E), \quad \mathbf{K}_{,i} = \tfrac{\partial \mathbf{K}}{\partial E_i}(E=\mu_E), \quad \mathbf{K}_{,ij} = \tfrac{\partial^2 \mathbf{K}}{\partial E_i \partial E_j}(E=\mu_E) \\ &\mathbf{u}_0 = \mathbf{u}(E=\mu_E), \quad \mathbf{u}_{,i} = \tfrac{\partial \mathbf{u}}{\partial E_i}(E=\mu_E), \quad \mathbf{u}_{,ij} = \tfrac{\partial^2 \mathbf{u}}{\partial E_i \partial E_j}(E=\mu_E) \end{aligned} \tag{17}$$

Note that the Taylor expansion of **F** does not appear here, since the expression of **F** does not contain E.

Substituting Eqs. (16a) and (16b) into Eq. (15) and collecting the terms of the same order yield

$$\begin{aligned} &\mathbf{K}_0\mathbf{u}_0 = \mathbf{F} \\ &\mathbf{K}_0\mathbf{u}_{,i} = -\mathbf{K}_{,i}\mathbf{u}_0 \\ &\mathbf{K}_0\mathbf{u}_{,ij} = -\mathbf{K}_{,ij}\mathbf{u}_0 - \mathbf{K}_{,i}\mathbf{u}_{,i} - \mathbf{K}_{,j}\mathbf{u}_{,j} \\ &\vdots \quad \vdots \quad \vdots \\ &\mathbf{u}_0 = \mathbf{K}_0^{-1}\mathbf{F} \\ &\mathbf{u}_{,i} = \mathbf{K}_0^{-1}\left(-\mathbf{K}_{,i}\mathbf{u}_0\right) \\ &\mathbf{u}_{,ij} = \mathbf{K}_0^{-1}\left(-\mathbf{K}_{,ij}\mathbf{u}_0 - \mathbf{K}_{,i}\mathbf{u}_{,i} - \mathbf{K}_{,j}\mathbf{u}_{,j}\right) \\ &\vdots \quad \vdots \quad \vdots \end{aligned} \quad \text{or} \tag{18}$$

Eq. (18) is the SSMLPG formulation of Eq. (1). Applying this equation follows four steps: (1) Compute **F** and $\mathbf{K}_0$ by setting $E_J = \mu_E$ (J = 1 to N_T); (2) Compute $\mathbf{u}_0 = \mathbf{K}_0^{-1}\mathbf{F}$; (3) Compute $\mathbf{K}_{,i}$, $\mathbf{K}_{,ij}$,….. using $E_J = \mu_E$ (J = 1 to N_T); and (4) Solve $\mathbf{u}_{,i}$, $\mathbf{u}_{,ij}$... by the resulting $\mathbf{u}_0$. In addition, with setting $E_J = \mu_E$ (J = 1 to N_T), any MLPG program can be used to complete the first three steps. An additional module can be appended to this MLPG package for solving $\mathbf{u}_{,i}$, $\mathbf{u}_{,ij}$....

Furthermore, observing Eq. (18) can understand that the stability of Eq. (18) depends upon whether $\mathbf{K}_{,i}$, $\mathbf{K}_{,ij}$,…. can be obtained. For the current study, obtaining $\mathbf{K}_{,i}$, $\mathbf{K}_{,ij}$,…. is easy, since only a linear elastic stress-strain relationship is introduced.

After accumulating the resulting $\mathbf{u}_0$, $\mathbf{u}_{,i}$, $\mathbf{u}_{,ij}$..., a first-order perturbation approximation of **u** is

$$\mathbf{u} = \mathbf{u}_0 + \sum_{i=1}^{N_T} \mathbf{u}_{,i}\Delta E_i \tag{19}$$

with the expected value: $\mathrm{Ex}[\mathbf{u}] = \mathbf{u}_0$ (20)

and the covariance matrix:

$$Cov[\mathbf{u},\mathbf{u}] = \mathrm{Ex}[(\mathbf{u}-\mathrm{Ex}[\mathbf{u}])(\mathbf{u}-\mathrm{Ex}[\mathbf{u}])^T] = \sum_{i=1}^{N_T}\sum_{j=1}^{N_T} \mathbf{u}_{,i}(\mathbf{u}_{,j})^T \mathrm{Ex}[\Delta E_i \Delta E_j] \tag{21}$$

in which $\mathrm{Ex}[\Delta E_i \Delta E_j]$ can be determined analytically by the autocorrelation function of E. In addition, a second-order perturbation approximation of **u** is

$$\mathbf{u} = \mathbf{u}_0 + \sum_{i=1}^{N_T} \mathbf{u}_{,i}\Delta E_i + \tfrac{1}{2}\sum_{i=1}^{N_T}\sum_{j=1}^{N_T} \mathbf{u}_{,ij}\Delta E_i \Delta E_j \tag{22}$$

with the expected value:

$$\mathrm{Ex}[\mathbf{u}] = \mathbf{u}_0 + \tfrac{1}{2}\sum_{i=1}^{N_T}\sum_{j=1}^{N_T} \mathbf{u}_{,ij}\mathrm{Ex}[\Delta E_i \Delta E_j] \tag{23}$$

and the covariance matrix:

$$\begin{aligned} Cov[\mathbf{u},\mathbf{u}] &= \sum_{i=1}^{N_T}\sum_{j=1}^{N_T} \mathbf{u}_{,i}(\mathbf{u}_{,j})^T \mathrm{Ex}[\Delta E_i \Delta E_j] \\ &+ \tfrac{1}{4}\sum_{i=1}^{N_T}\sum_{j=1}^{N_T}\sum_{k=1}^{N_T}\sum_{l=1}^{N_T} \mathbf{u}_{,ij}(\mathbf{u}_{,ij})^T \begin{Bmatrix} \mathrm{Ex}[\Delta E_i \Delta E_l]\mathrm{Ex}[\Delta E_j \Delta E_k] \\ +\mathrm{Ex}[\Delta E_i \Delta E_k]\mathrm{Ex}[\Delta E_j \Delta E_l] \end{Bmatrix} \end{aligned} \tag{24}$$

In addition, observing Eqs. (19) and (22) can understand that the posterior errors of perturbation method are caused by truncating $\mathbf{u}_{,ijk}$, $\mathbf{u}_{,ijkL}$…(i, j, k, L = 1 to N_T) in equating these two equations. Additionally computing these $\mathbf{u}_{,ijk}$, $\mathbf{u}_{,ijkL}$… can estimate those posterior errors.

4. RESULTS

Implement the performance evaluation of proposed perturbation-based SSMLPG formulation through a stochastic elastostatic problem in which a strip loading bears on a field foundation clay layer. As a comparison, an SSFEM package FERUM [9] is additionally applied to this stochastic elastostatic problem. Eqs. (19), (22) and the FERUM package are used to predict Ex[**u**] and standard deviation Std[**u**] with the uncertainty in the spatial variability of E. Note that the FERUM package does not include any module for compute the perturbation expansion of a random field. Therefore, an additional module is appended to the FERUM package for providing the perturbation-based SSFEM results.

For simplicity, the performance evaluation of perturbation-based SSMLPG formulation focuses on three aspects:

a. Comparing the agreements between the MCS and SSMLPG or SSFEM results.

b. Evaluating the influence of the spatial variability of E on the agreements between the MCS and SSMLPG results.

c. Studying the agreements between the MCS and SSMLPG results when discrete nodes are used.

Fig. (**2**) displays the layout of Ω and boundary conditions in which B is the half of foundation width, H is the thickness of the clay layer, and σ_0 is the magnitude of the foundation loading. In addition, assume the spatial variability of E follows two probabilistic distributions (named by Distributions A and B). The first probabilistic distribution is

$$E = \mu_E[1 + \alpha(\mathbf{x})] \tag{25}$$

where μ_E is independent of **x** and $\alpha(\mathbf{x})$ is a zero-mean, scalar, homogeneous random field with its autocorrelation function $\Gamma_\alpha(\boldsymbol{\xi})$ equal to

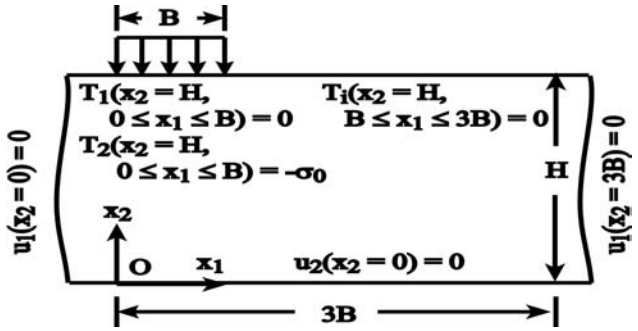

Fig. (2). Benchmark problem for implementing a performance evaluation of the perturbation-based SSMLPG formulation (not to scale).

$$\text{(Distribution A)}\ \ \Gamma_\alpha(\boldsymbol{\xi}) = S_E^2 \exp\left[-\left(\frac{|\xi_1|}{b_1 B} + \frac{|\xi_2|}{b_2 H}\right)\right] \tag{26}$$

where b_1 and b_2 are two constants, S_E is the standard deviation of E, $(\xi_1, \xi_2) = \mathbf{x}_2 - \mathbf{x}_1$, and $\mathbf{x}_i$, i = 1 to 2 are two nodes. Based on Eq. (26), $Ex[\Delta E_i \Delta E_j]$ is derived by

$$Ex[\Delta E_i \Delta E_j] = S_E^2 \exp\left[-\left(\frac{|x_{i,1}-x_{j,1}|}{b_1 B} + \frac{|x_{i,2}-x_{j,2}|}{b_2 H}\right)\right] \tag{27}$$

where $x_{i,1}$ and $x_{i,2}$ are the components of $\mathbf{x}_i$, $x_{j,1}$ and $x_{j,2}$ are the components of $\mathbf{x}_j$. Similarly manipulating Eq. (27) can obtain $Ex[\Delta E_i \Delta E_l]$, $Ex[\Delta E_j \Delta E_k]$, $Ex[\Delta E_i \Delta E_k]$, and $Ex[\Delta E_j \Delta E_l]$.

The second probability distribution is similar to Eq. (25) except that $\Gamma_\alpha(\boldsymbol{\xi})$ is

$$\text{(Distribution B)}\ \ \Gamma_\alpha(\boldsymbol{\xi}) = S_E^2 \left(1 - \frac{|\xi_1|}{b_1 B}\right)\left(1 - \frac{|\xi_2|}{b_2 H}\right) \tag{28}$$

Based on Eq. (28), $Ex[\Delta E_i \Delta E_j]$ is re-derived by

$$Ex[\Delta E_i \Delta E_j] = S_E^2 \left(1 - \frac{|x_{i,1}-x_{j,1}|}{b_1 B}\right)\left(1 - \frac{|x_{i,2}-x_{j,2}|}{b_2 H}\right) \tag{29}$$

However, since E varies according to a random field $\alpha(\mathbf{x})$, the analytical solutions of **u** don't exist. We should generate an MCS to provide the standard for comparing the SSMLPG and SSFEM results. Implementing an MCS requires three steps: (a) Generate a number of samples of E according to Eq. (26) or (28); and (b) Substitute each sample of E into Eq. (15) and the FERUM package to predict **u**. (c) Compute Ex[**u**] and Std[**u**] values of the resulting **u**. If the total number of samples of E is sufficiently large, the resulting Ex[**u**] and Std[**u**] values approach their exact values (but are still not exact values). Such Ex[**u**] and Std[**u**] values can be the standard for comparing the SSFEM-based and SSMLPG-based predicted Ex[**u**] and Std[**u**]. Essential parameters for this comparison are listed below

a. Set σ_0 = 1 kN/m^2, ν = 0.3, B = 10 m, and H = 4.3 m. Define Ω as $0 \le x_1 \le 3B$ and $0 \le x_2 \le H$. Generate 15000 samples of E to implement an MCS. Adopt 16 quadrature points in calculating the numerical integration over an Ω_S.

b. Set α_c = 4.0, q = 1.03, and d_c = 3.0 in computing the MQ RBF. These α_c, q, and d_c values come from a published reference [10] in which the most proper α_c, q, and d_c values for applying this MQ RBF are studied. As a consequence, setting α_c = 4.0, q = 1.03, and d_c = 3.0 results in satisfactory interpolation errors.

c. Intentionally choose a complete monomial basis of order 3 to construct ϕ. Observe the agreement between the corresponding MCS and SSMLPG results with respect to such a lower order value.

d. Choose Ω_Q for any point as a circle centered at this point. Set the radius of each Ω_Q equal to 2.58 m. Choose Ω_S for a node as a rectangle centered at this node. Set the width and length of each Ω_S both equal to 2.58 m. Such sizes of Ω_Q and Ω_S are set according to a previous study [10] and a pilot test evaluating the time spent to complete an MCS. Accordingly, the size of Ω_Q or Ω_S should be larger than 1.5 times the spacing of any two connecting nodes for obtaining less interpolation errors [10]. Meanwhile, the pilot test identified the time spent to complete an MCS using 15000 samples is acceptable[1].

e. Generate two cases (named by Discretizations A and B) of meshless discretization. Fig. (**3a**, **b**) illustrate these two cases of the meshless discretization. Fig. (**3c**) shows the finite element discretization for executing the FERUM package.

f. Define the accuracy standard is $\varepsilon\{Ex[u_i]\} \le 10$ %, $\varepsilon\{Std[u_i]\} \le 10$ %, $\Delta\{Ex[u_i]\} \le 10$ %, and $\Delta\{Std[u_i]\} \le 10$ % where $Ex[u_i]$ and $Std[u_i]$ are; respectively, the components of Ex[**u**] and Std[**u**], ε and Δ are the error estimators quantifying the agreements between MCS and SSMLPG or SSFEM results. ε and Δ are defined by

$$\varepsilon\{Ex[u_i]\}(\%) = \left|\frac{Ex[u_i]_{MCS} - Ex[u_i]_{SSMLPG}}{Ex[u_i]_{MCS}}\right|,\ \varepsilon(Std[u_i])(\%) = \left|\frac{Std[u_i]_{MCS} - Std[u_i]_{SSMLPG}}{Std[u_i]_{MCS}}\right| \tag{30a}$$

$$\Delta\{Ex[u_i]\}(\%) = \left|\frac{Ex[u_i]_{MCS} - Ex[u_i]_{SSFEM}}{Ex[u_i]_{MCS}}\right|,\ \Delta\{Std[u_i]\}(\%) = \left|\frac{Std[u_i]_{MCS} - Std[u_i]_{SSFEM}}{Std[u_i]_{MCS}}\right| \tag{30b}$$

In Eqs. (30a) and (30b) $Ex[u_i]_{MCS}$ and $Std[u_i]_{MCS}$ are computed by

$$Ex[u_i] = \frac{1}{N_s}\sum_{j=1}^{N_s} u_{i,j},\ Std[u_i] = \sqrt{\frac{1}{N_s}\sum_{j=1}^{N_s}\left\{u_{i,j} - Ex[u_i]\right\}^2} \tag{31}$$

[1]Using an Intel® Core™ 2 Duo CPU.

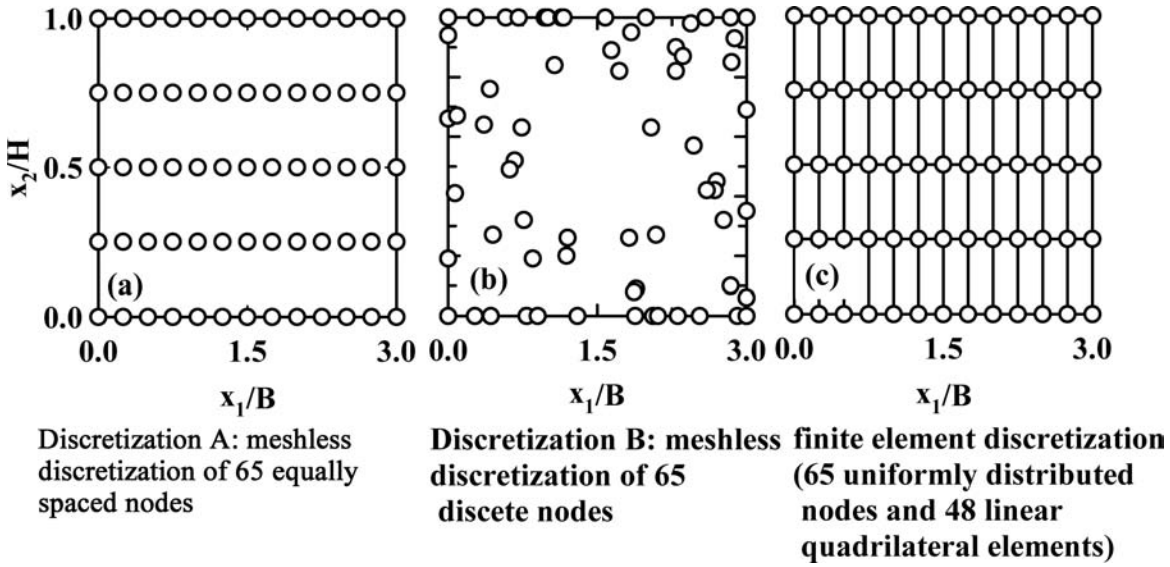

Fig. (3). Meshless and finite element discretizations for analyzing the benchmark problem (not to scale).

where, N_s is the total number of samples of **u**, and the subscript j denotes the j-th sample of E. In addition, $Ex[u_i]_{SSMLPG}$ and $Ex[u_i]_{SSFEM}$ can be calculated by Eq. (20) or (23). However, $Std[u_i]_{SSMLPG}$ and $Std[u_i]_{SSFEM}$ are computed by

$$Var(\mathbf{u}) = diag\{Cov[\mathbf{u},\mathbf{u}]\},\ Std[u_i] = \sqrt{Var(u_i)} \tag{32}$$

where Var(**u**) is the variance of **u**, $Var(u_i)$ are its components, and diag is the diagonals of Cov[**u**,**u**].

Agreements Between the Monte Carlo Simulation and Spectral Stochastic Meshless Local Petrov-Galerkin Results

Figs. (**4a-d**, **5a-d**) compare variation of $\varepsilon(Ex[u_i])$, $\varepsilon(Std[u_i])$, $\Delta(Ex[u_i])$, and $\Delta(Std[u_i])$ (i = 1 to 2) with respect to x_i. Table **1** further lists the ranges of $\varepsilon(Ex[u_i])$, $\varepsilon(Std[u_i])$, $\Delta(Ex[u_i])$, and $\Delta(Std[u_i])$.

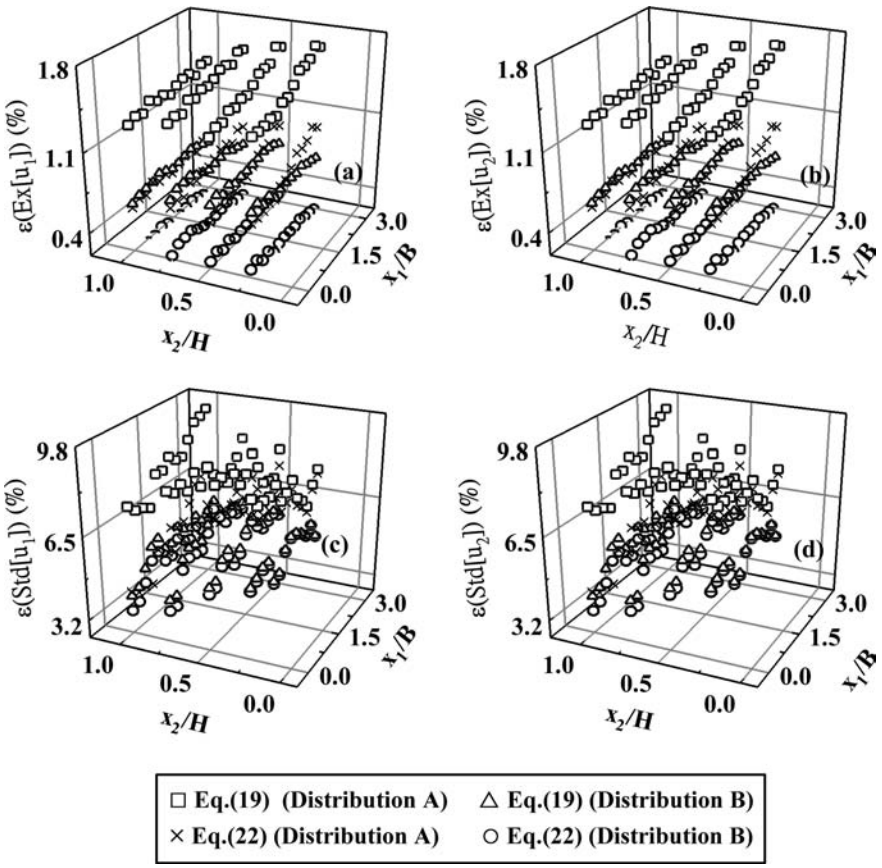

Fig. (4). Variation of $\varepsilon(Ex[u_i])$ and $\varepsilon(Std[u_i])$ (i = 1 to 2) versus x_i (Discretization A, $S_E/\mu_E = 0.12$, $b_1 = b_2 = 1$, $N_s = 15000$).

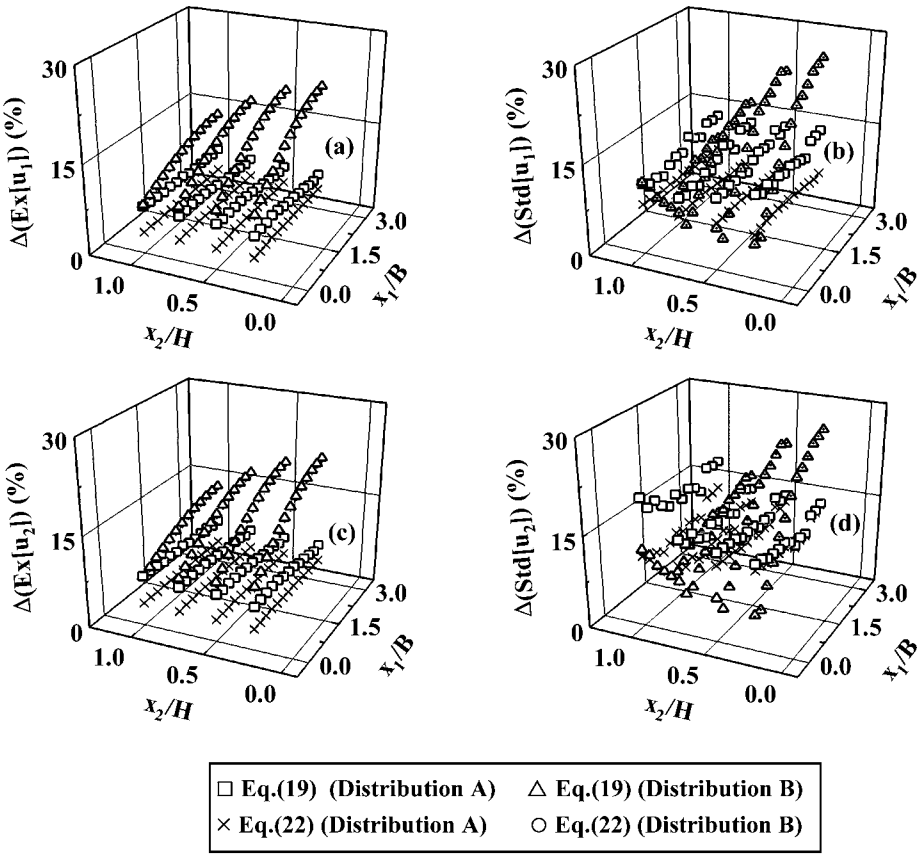

Fig. (5). Variation of $\Delta(Ex[u_i])$ and $\Delta(Std[u_i])$ (i = 1 to 2) versus x_i ($S_E/\mu_E = 0.12$, $b_1 = b_2 = 1$, $N_s = 15000$).

Table 1. Ranges of $\varepsilon(Ex[u_i])$, $\varepsilon(Std[u_i])$, $\Delta(Ex[u_i])$ and $\Delta(Std[u_i])$ (i = 1 to 2)

		$\varepsilon(Ex[u_1])$	$\varepsilon(Ex[u_2])$	$\varepsilon(Std[u_1])$	$\varepsilon(Std[u_2])$	$\Delta(Ex[u_1])$	$\Delta(Ex[u_2])$	$\Delta(Std[u_1])$	$\Delta(Std[u_2])$
1st-order (%)	Distribution A	1.31 ~ 1.72	1.3 ~ 1.71	6.49 ~ 9.43	6.49 ~ 9.44	5.97 ~ 7.92	6.23 ~ 8.28	12.1 ~ 22.1	10.7 ~ 20.8
	Distribution B	0.63 ~ 0.82	0.62 ~ 0.81	4.03 ~ 6.73	4.02 ~ 6.73	8.13 ~ 21.4	8.13 ~ 21.3	4.1 ~ 26	4.44 ~ 26.1
2nd-order (%)	Distribution A	0.59 ~ 1.01	0.6 ~ 1.01	3.84 ~ 8.08	3.85 ~ 8.09	3.38 ~ 3.86	3.48 ~ 3.95	9.89 ~ 14.6	9.41 ~ 13.7
	Distribution B	0.13 ~ 0.32	0.12 ~ 0.31	3.42 ~ 6.41	3.42 ~ 6.41	7.65 ~ 21	7.64 ~ 20.9	4.03 ~ 21	4.03 ~ 22.1

Surprisingly, Fig. (**4a-d**) identify that $\varepsilon(Ex[u_i])$ and $\varepsilon(Std[u_i])$ computed based on Eq. (19) satisfy the accuracy standard. In addition, comparing Table **1**, Figs. (**4a-d**, **5a-d**) indicates that the SSMLPG results approach more closely to the MCS results than the SSFEM results do, since $\varepsilon(Ex[u_i])$ and $\varepsilon(Std[u_i])$ are; respectively, less than $\Delta(Ex[u_i])$ and $\Delta(Std[u_i])$. Note that generating the SSMLPG results spends about 300 seconds; while completing the MCS requires about 1.5 hr.

Influence of the Spatial Variability of Young's Modulus on the Spectral Stochastic Meshless Local Petrov-Galerkin Results

Discuss first the necessity of accounting for the spatial variability of E in predicting **u**. As an example, Fig. (**6a**, **b**) display variation of $u_i(x_2 = H \wedge 0 \le x_1 \le 3B)/H$ (i = 1 to 2) *vs* x_1 with and without accounting for the spatial variability of E. In these two figures, **u** is predicted by Eq. (19).

As compared to SSMLPG-based predicted $u_1(x_2 = H)/H$, Fig. (**6a**, **b**) demonstrate that SSMLPG-based predicted $u_2(x_2 = H)/H$ varies within a wider range. As a consequence, obtaining unreliable predicted $u_2(x_2 = H)$ is more possible than obtaining unreliable predicted $u_1(x_2 = H)$, if the spatial variability of E is neglected.

Next, study the influence of different spatial variability of E on the accuracy of SSMLPG results. Since Eqs. (26) and (28) show that adjusting the spatial variability of E is equivalent to using different b_1, b_2, and S_E values, we turn to study the influence of different b_1, b_2, and S_E values on the agreements between the MCS and SSMLPG results. Fig. (**7a**, **b**) show variation of $\varepsilon(Ex[u_i])$ and $\varepsilon(Std[u_i])$ (i = 1 to 2) *vs* x_i, $b_1 = 1$, and $b_2 = 2$. Fig. (**8a**, **b**) show variation of

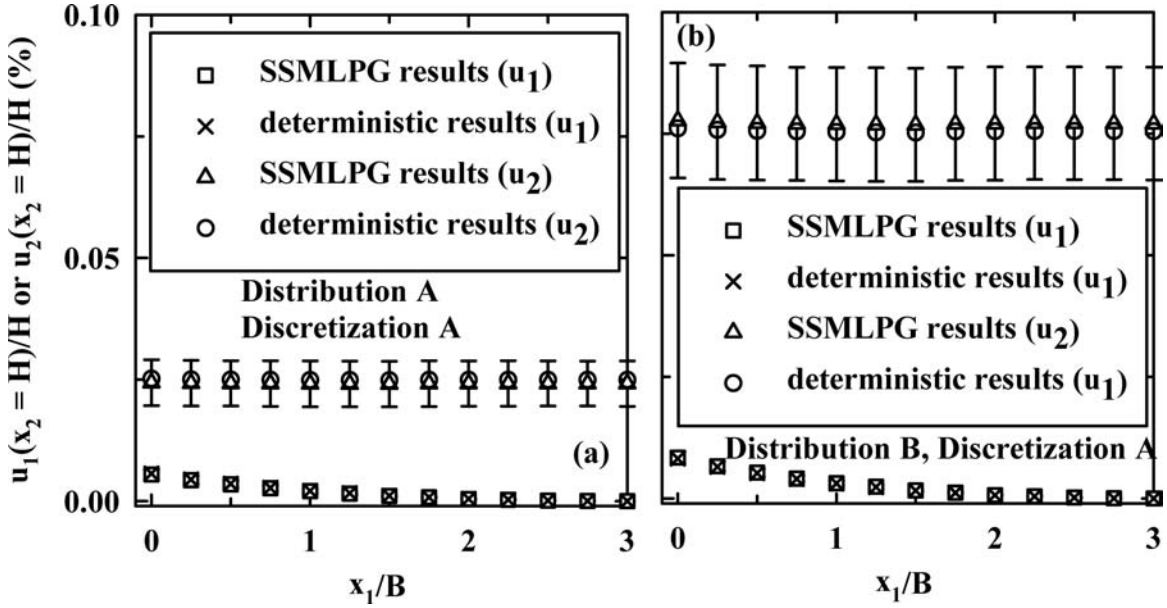

Fig. (6). Comparison of predicted $\mathbf{u}(x_2 = H \wedge 0 \leq x_1 \leq 3B)/H$ with and without accounting for the uncertainty contributed by the spatial variability of E (using Eq. (19)).

$\varepsilon(Ex[u_i])$ and $\varepsilon(Std[u_i])$ *vs* x_i and $S_E/\mu_E = 0.24$. In these four figures, **u** is computed by Eq. (22).

Comparing Figs. (**4c**, **d**, **7a**, **b**) identifies that $\varepsilon(Ex[u_i])$ and $\varepsilon(Std[u_i])$ values decrease when b_2 values increase. Comparing Figs. (**4c**, **d**, **8a**, **b**) indicates that doubling the S_E value increases the $\varepsilon(Ex[u_i])$ and $\varepsilon(Std[u_i])$ values. In Fig. (**8a**, **b**), $\varepsilon(Ex[u_i])$ values still satisfy the accuracy standard, whereas some of $\varepsilon(Std[u_i])$ values don't.

Spectral Stochastic Meshless Local Petrov-Galerkin Results *vs* Discrete Nodes

Using Eq. (22) and Discretization B, Fig. (**9a**, **b**) display variation of $\varepsilon(Ex[u_i])$ and $\varepsilon(Std[u_i])$ (i = 1 to 2) *vs* x_i. These two figures indicate that the proposed perturbation-based SSMLPG formulation can provide sufficiently accurate numerical results, even if nodes are randomly distributed. $\varepsilon(Ex[u_i])$ and $\varepsilon(Std[u_i])$ values in Fig. (**9a**, **b**) satisfy the accuracy standard.

5. DISCUSSIONS AND CONCLUSION

This study presents an SSMLPG formulation containing perturbation expansions of random fields and a 2D MWS formulation in elasticity. In Sec.4, the performance of this SSMLPG formulation is evaluated. Some discussions are drawn from the evaluation results:

a. Even if the first-order perturbation approximation of **u** is used, Fig. (**4a-d**) show that SSMLPG-based predicted Ex[**u**] and Std[**u**] are still sufficiently

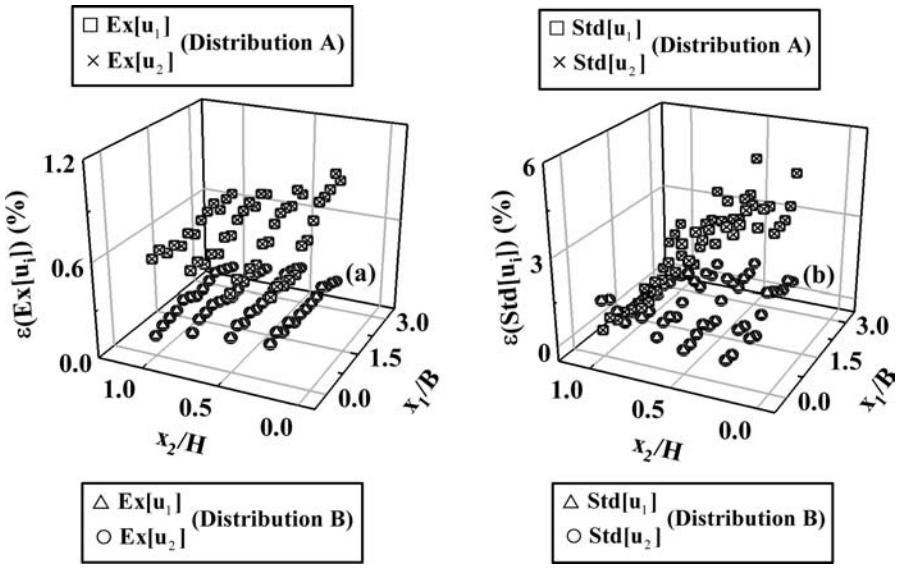

Fig. (7). Variation of $\varepsilon(Ex[u_i])$ and $\varepsilon(Std[u_i])$ (i = 1 to 2) versus $x_i$and $b_1 = 1$, $b_2 = 2$ (Using Eq. (22) Discretization B, $S_E/\mu_E = 0.12$, and $N_s = 15000$).

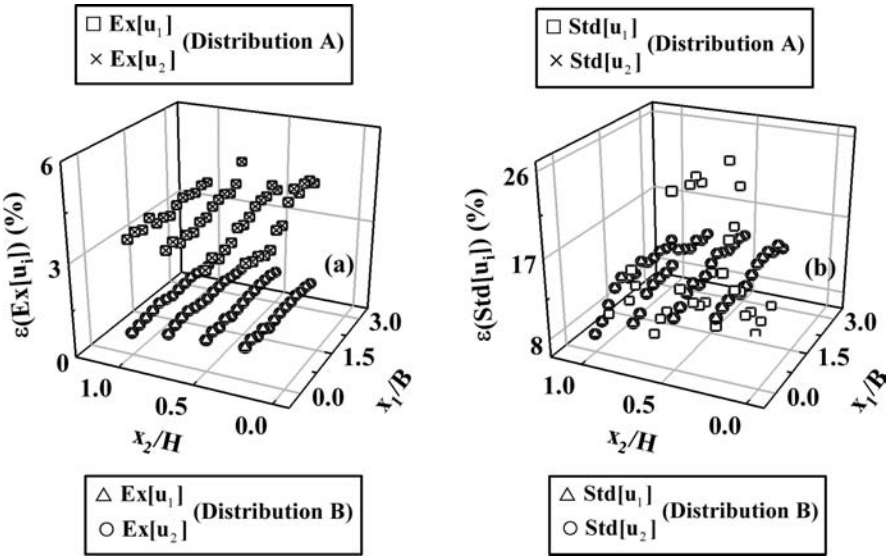

Fig. (8). Variation of ε(Ex[u_i]) and ε(Std[u_i]) (i = 1 to 2) with respect to x_i and $S_E/\mu_E = 0.24$ (Using Eq. (22) Discretization A, $b_1 = b_2 = 1$, and $N_s = 15000$).

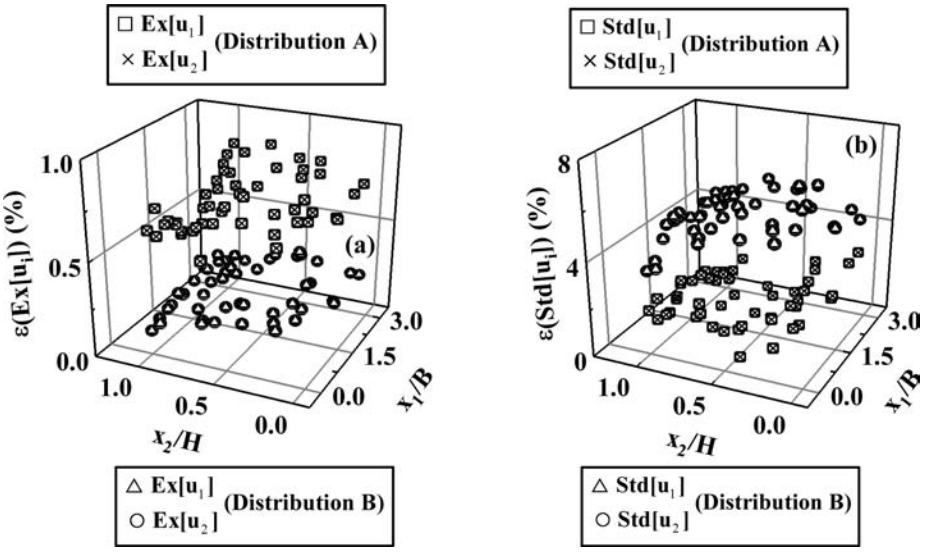

Fig. (9). Variation of ε(Ex[u_i]) and ε(Std[u_i]) (i = 1 to 2) versus x_i (Using Eq. (22) Discretization B, $S_E/\mu_E = 0.12$, $b_1 = b_2 = 1$, and $N_s = 15000$).

accurate. Such experience was not mentioned in applying other stochastic numerical methods. For example, a previous study [11] concluded that the accuracy of stochastic element-free Galerkin (SEFGM)-based predicted Ex[**u**] and Std[**u**] is unsatisfactory, if the first-order perturbation approximation of **u** is used. Consequently, Fig. (**4a-d**) encourage the further application of perturbation-based SSMLPG formulation to three-dimensional problems. Solving a three-dimensional problem is usually time-consuming; whereas computing the first-order perturbation approximation is time-saving. If using the first-order perturbation approximation of **u** can result in sufficiently accurate predicted Ex[**u**] and Std[**u**], we are more willing to apply the SSMLPG method to three-dimensional problems.

b. Comparing Fig. (**4a-d**) with Fig. (**5a-d**) identifies that the SSMLPG results approach more closely to the MCS results than the SSFEM results do. The better accuracy of SSMLPG results may attribute to the difference between meshfree and finite element shape functions, since other parameters for plotting Figs. (**4a-d**, **5a-d**) are almost identical. Nevertheless, further applying the SSMLPG and SSFEM methods to other types of stochastic boundary-value problems is suggested.

c. Figs. (**7a**, **b**, **8a**, **b**) show that b_1, b_2, and S_E values do affect the accuracy of SSMLPG results. To obtain more proper b_1, b_2, and S_E values, we may compute different b_1, b_2, and S_E values for each Ω_Q. Such an idea can be tested in solving a practical stochastic boundary-value problem. The SSMLPG method gives

more freedom to support this idea, since each Ω_Q is arbitrary. We can freely adjust any Ω_Q but fix other Ω_Q for obtaining more proper b_1, b_2, and S_E values.

d. Fig. (**9a**, **b**) display that the proposed perturbation-based SSMLPG formulation still provides satisfactory numerical results when discrete nodes are used. Such performance facilitates solving practical stochastic boundary-value problems. In a practical stochastic boundary-value problem, data of material properties are measured at discrete nodes. The SSMLPG method can directly incorporate with such data to produce sufficiently accurate numerical results. If the SSFEM and SEFGM methods are applied for the same stochastic boundary-value problem, additional nodes are required to create a finite element discretization or background cells.

In conclusion, the SSMLPG method can be an efficient alternative for solving stochastic boundary-value problems.

ACKNOWLEDGEMENT

Declared none.

CONFLICT OF INTEREST

Declared none.

REFERENCES

[1] Ghanem RG, Spanos PD. Stochastic finite elements: a spectral approach. New York: Springer 1981.

[2] Wu SQ, Law SS. Dynamic analysis of bridge with non-Gaussian uncertainties under a moving vehicle. Probab Eng Mech 2011; 26(2): 281-93.

[3] Ngah MF, Young A. Application of the spectral stochastic finite element method for performance prediction of composite structures. Compos Struct 2007; 78(3): 447-56.

[4] Kim HK, Inoue J. A spectral stochastic element free Galerkin method for the problems with random material parameter. Int J Numer Methods Eng 2004; 61(11): 1957-75.

[5] Sheu GY. Prediction of probabilistic settlements *via* spectral stochastic meshless local Petrov-Galerkin method. Comput Geotech 2011; 38(4): 407-15.

[6] Atlrui SN, Zhu T. A new meshless local Petrov-Galerkin (MLPG) approach in computational mechanics. Comput Mech 1988; 22(2): 117-27.

[7] Liu GR, Gu YT. A meshfree method: meshfree weak-strong (MWS) form method, for 2-D solids. Comput Mech 2004; 33(1): 2-14.

[8] Kaminski, M. Generalized perturbation-based stochastic finite element in elastostatics. Comput Struct 2007; 85(10): 586-94.

[9] Sudret B, Kiureghian AD. Stochastic finite elements and reliability: a state-of-the-art report. Technical Report 2000, UCB/SEMM-2000/08. Berkeley: University of California 2000.

[10] Liu GR. Meshfree methods: moving beyond the finite element method. Boca Raton, USA: CRC press 2002.

[11] Rahman S, Rao BN. A perturbation method for stochastic meshless analysis in elastostatics. Int J Numer Methods Eng 2001; 50(8): 1969-91.

Received: November 18, 2011 Revised: December 4, 2011 Accepted: December 6, 2011